GEOPHYSICS, VOL. 65, NO. 6 (NOVEMBER-DECEMBER 2000); P. 1920–1930, 7 FIGS.

Radio tomography and borehole radar delineation of the McConnell nickel sulfide deposit, Sudbury, Ontario, Canada

Peter K. Fullagar*, Dean W. Livelybrooks‡, Ping Zhang**, Andrew J. Calvert§, and Yiren Wu§§

ABSTRACT

In an effort to reduce costs and increase revenues at mines, there is a strong incentive to develop high-resolution techniques both for near-mine exploration and for delineation of known orebodies. To investigate the potential of high-frequency EM techniques for exploration and delineation of massive sulfide orebodies, radio frequency electromagnetic (RFEM) and ground-penetrating radar (GPR) surveys were conducted in boreholes through the McConnell massive nickel–copper sulfide body near Sudbury, Ontario, from 1993–1996.

Crosshole RFEM data were acquired with a JW-4 electric dipole system between two boreholes on section 2720W. Ten frequencies between 0.5 and 5.0 MHz were recorded. Radio signals propagated through the Sudbury Breccia over ranges of at least 150 m at all frequencies. The resulting radio absorption tomogram clearly imaged the McConnell deposit over 110 m downdip. Signal was extinguished when either antenna entered the sulfide body. However, the expected radio shadow did not eventuate when transmitter and receiver were on opposite sides of the deposit. Two-dimensional modeling suggested that diffraction around the edges of the sulfide body could not account for the observed field amplitudes. It was concluded at the time that the sulfide body is discontinuous; according to modeling, a gap as small as 5 m could have explained the observations. Subsequent investigations by INCO established that pick-up in the metal-cored downhole cables was actually responsible for the elevated signal levels.

Both single-hole reflection profiles and crosshole measurements were acquired using RAMAC borehole radar systems, operating at 60 MHz. Detection of radar reflections from the sulfide contact was problematic. One coherent reflection was observed from the hanging-wall contact in single-hole reflection mode. This reflection could be traced about 25 m uphole from the contact. In addition to unfavorable survey geometry, factors which may have suppressed reflections included host rock heterogeneity, disseminated sulfides, and contact irregularity.

Velocity and absorption tomograms were generated in the Sudbury Breccia host rock from the crosshole radar. Radar velocity was variable, averaging 125 m/μs, while absorption was typically 0.8 dB/m at 60 MHz. Kirchhoff-style 2-D migration of later arrivals in the crosshole radargrams defined reflective zones that roughly parallel the inferred edge of the sulfide body.

The McConnell high-frequency EM surveys established that radio tomography and simple radio shadowing are potentially valuable for near- and in-mine exploration and orebody delineation in the Sudbury Breccia. The effectiveness of borehole radar in this particular environment is less certain.

INTRODUCTION

Borehole EM methods are being applied increasingly in and near metalliferous mines for both exploration and orebody delineation. In the context of near-mine exploration for base metals, downhole transient EM methods such as UTEM have proved effective for detecting deep orebodies at ranges of hundreds of meters from boreholes (e.g., King, 1996). At the same

Manuscript received by the Editor May 10, 1999; revised manuscript received June 16, 2000.
*Fullagar Geophysics Pty. Ltd., Level 1, 1 Swann Road, Taringa, Queensland 4068, Australia. E-mail: p.fullagar@mailbox.uq.edu.au.
‡University of Oregon 1274, Department of Physics, Eugene, Oregon 97403-1274. E-mail: dlivelyb@hendrix.uoregon.edu.
**Electromagnetics Instruments, Inc., P.O. Box 463, El Cerrito, California 94530-0463.
§Simon Fraser University, Department of Earth Sciences, 8888 University Drive, Burnaby, British Columbia V5A 1S6, Canada.
§§Beijing Xin Yi Hightech Research Institute 70 Bei Lishi Road, Beijing 100037, China.

time the drive for more efficient mine production techniques to reduce costs and increase revenues has stimulated interest in high-frequency borehole EM techniques. Radio imaging and ground-penetrating radar (GPR) methods show particular promise for orebody delineation.

The use of radio waves to define geological features between boreholes can be traced back to a 1910 German patent (Thomson and Hinde, 1993). Radio tomography (RT) per se was pioneered by Lager and Lytle (1977) and has since been applied extensively to detect faults and other disruptions in the continuity of seams of coal or potash (McGaughey and Stolarczyk, 1991; Vozoff et al., 1993). The utility of radio imaging in metalliferous exploration and mining is currently under investigation. Radio frequency methods in the 10 kHz to 1 MHz band have already enjoyed some success in this context, e.g., Nickel and Cerny (1989), Anderson and Logan (1992), Thomson et al. (1992), Wedepohl (1993), Zhou et al. (1998), and Stevens and Redko (2000). RT can deliver higher resolution than traditional borehole EM systems, both by virtue of its higher frequencies and because the radio transmitter can be lowered down a borehole, closer to the target.

GPR detects changes in permittivity and conductivity using high-frequency electromagnetic pulses (10 MHz–1 GHz). Conventional GPR has found application in underground coal mines (Coon et al., 1981; Yelf et al., 1990) and is used routinely to define auriferous zones in the Witwatersrand (Campbell, 1994) and at the Sixteen to One mine in California (Raadsma, 1994). Other mining applications include mapping conductive salt structures (Stewart and Unterberger, 1976), exploring for placer deposits (Davis et al., 1985), detecting geotechnical hazards (Fullagar and Livelybrooks, 1994a), and delineating lateritic deposits. Borehole radar is well established in salt and potash mines (Mundry et al., 1983; Eisenburger et al., 1993; Thierbach, 1994), but application in nonevaporite mines is still relatively uncommon, notwithstanding the strong commercial incentive to accurately define ore boundaries and structures. Encouraging experimental applications of borehole reflection radar have been reported from coal mines (Murray et al., 1998), Witwatersrand gold mines (Wedepohl et al., 1998), and base metal sulfide mines (Liu et al., 1998; Zhou and Fullagar, 2000).

This article summarizes activities undertaken at the McConnell nickel sulfide deposit from 1993–1996 by a research group formed under the NSERC/TVX Gold/Golden Knight Chair in Borehole Geophysics for Mineral Exploration at Ecole Polytechnique, Montreal. Borehole radar trials were performed with a 22-MHz RAMAC I system in December 1993 (Fullagar and Livelybrooks, 1994b; Stevens and Lodha, 1994) and with a 60-MHz RAMAC LI system in June 1996 (Calvert and Livelybrooks, 1997). Both single-hole reflection and crosshole data were recorded. A radio imaging survey was undertaken in April 1994 with a JW-4 electric dipole system (Fullagar et al., 1996). Data were recorded at ten frequencies between 0.5 and 5.0 MHz.

The McConnell deposit, owned by INCO Ltd., is located near Garson mine on the southeastern rim of the Sudbury basin, Ontario, Canada. It is a tabular body of massive sulfides (pentlandite–pyrrhotite), about 200 m along strike, 300 m downdip, and averaging 15 m true thickness (Figure 1). The mineralization is hosted by a quartz diorite dyke, intruded into heterogeneous Sudbury Breccia country rock, comprised of blocks of metavolcanics and metasediments. The dyke strikes 85° east and dips 70° south.

The McConnell sulfide body is shallow, extensively drilled, and close to an operating mine, rendering it an excellent geophysical test site. Prior to the work described here, the Geological Survey of Canada (GSC) had recorded a comprehensive suite of downhole geophysical logs at McConnell (Mwenifumbo et al., 1993; Killeen et al., 1996). The dc resistivities varied over four orders of magnitude, from near zero in the massive sulfides to over 30 000 ohm-m within the breccia. The high resistivities of the host rocks rendered them favorable for propagation of EM waves, while the high conductivity of the massive sulfide body was expected to produce

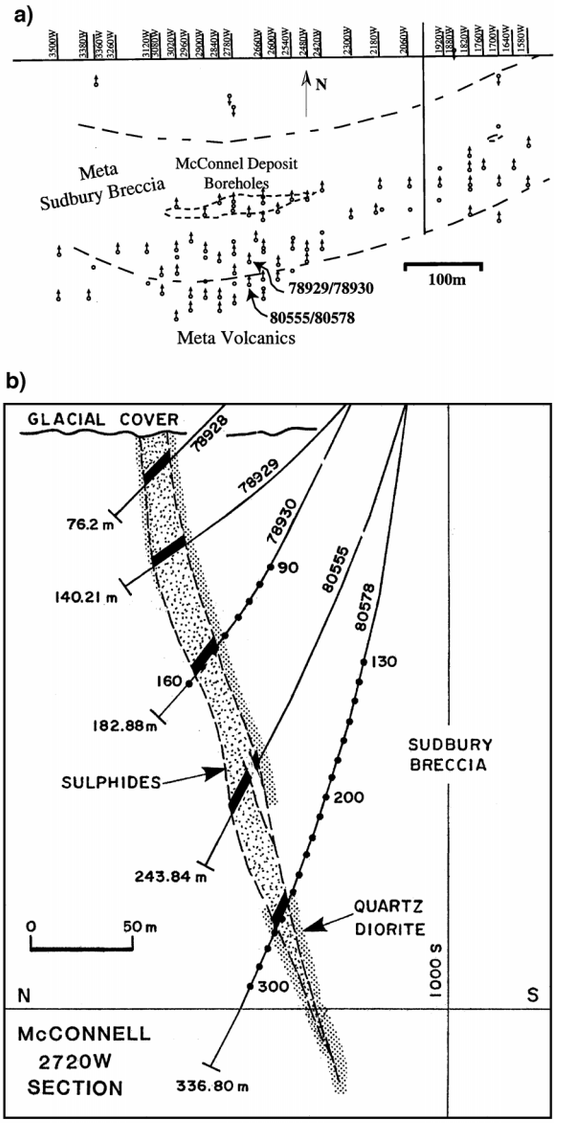

FIG. 1. McConnell deposit shown (a) in plan and (b) on section 2720W. Top of the sulfide body has been projected to the surface in (a). Transmitter locations for the RT survey are marked with dots in (b); thick black lines mark massive sulfide intersections. Westings in (a) are in feet; depths in (b) are in meters.

strong radar reflections and to create radio shadow zones. The McConnell site therefore represented an ideal location to assess the efficacy of radio tomography and borehole radar for delineating a known massive sulfide body.

THEORY

For EM waves propagating at angular frequency ω through a homogeneous isotropic medium with conductivity σ, real permittivity ε_r, and permeability μ, the real and imaginary parts, β and α, of the complex wavenumber k can be written as (Cook, 1975)

$$\beta = \omega\sqrt{\frac{\mu\varepsilon_r}{2}}(\sqrt{1+Q^{-2}}+1)^{1/2} \tag{1}$$

and

$$\alpha = \omega\sqrt{\frac{\mu\varepsilon_r}{2}}(\sqrt{1+Q^{-2}}-1)^{1/2}. \tag{2}$$

The value Q is the ratio of displacement current to conduction current,

$$Q = \frac{\omega\varepsilon_r}{\sigma_e}, \tag{3}$$

where σ_e is the effective conductivity (Turner and Siggins, 1994),

$$\sigma_e = \sigma + \omega\varepsilon_i, \tag{4}$$

with ε_i denoting the imaginary part of permittivity.

The scalar wavenumber β determines the wavelength, while the absorption coefficient α controls attenuation. For both radio imaging and GPR surveys, the effective range increases with decreasing frequency, but at the expense of resolution. Thus, any survey involves a trade-off between resolution and range.

Radio imaging involves propagation of monofrequency EM signals in the 1 kHz to 10 MHz band between boreholes or mine accessways. In a typical crosshole RT survey, the transmitter is fixed in one hole while signal amplitude (and perhaps phase) is recorded at successive receiver stations in one or more other holes. Signals which are weak and retarded in phase are indicative of more conductive material between the transmitter and receiver. Tomographic reconstruction of the signal amplitudes and phases at all receiver stations provides an image of the conductivity distribution between the boreholes.

GPR involves emission, propagation, and detection of EM pulses, with center frequencies usually between 10 MHz and 1 GHz. GPR can be deployed in transmission mode, like radio imaging, but it is more commonly applied in reflection mode. In the latter case it is closely analogous to the seismic reflection method. GPR can map contrasts in electrical properties or fluid content which usually coincide with geological contacts and structures. Radar reflection coefficients depend on permittivity, conductivity, and permeability contrasts.

Most radar surveys are carried out under low-loss conditions ($Q \gg 1$), for which the propagation involves polarization of the medium. Typical rocks are characterized by relative dielectric constants between 3 and 30. The presence of water, with its large relative dielectric constant (~80), serves to dramatically retard propagating waves.

The demarkation between GPR and RFEM applications is not sharp, but generally radio imaging is used at frequencies between 1 kHz and 10 MHz, often in lossy (low Q) environments. RFEM equipment can operate effectively in the diffusion domain $Q \leq 1$, where conduction currents are at least comparable to, and often much larger than, displacement currents. In the limit of low Q, α and β assume the same functional form:

$$\alpha = \beta = \sqrt{\frac{\omega\mu\sigma_e}{2}}. \tag{5}$$

McCONNELL RADIO FREQUENCY EM SURVEY

RFEM data acquisition

Tomographic radio frequency surveys were undertaken between boreholes 80 578 and 78 930 in April 1994 using a JW-4 borehole radio imaging system developed by the Chinese Ministry of Geology and Mineral Resources (MGMR). The JW-4 is an electric field system, capable of recording axial component amplitude over a programmable sweep of frequencies between 0.5 and 32 MHz (Qu et al., 1991). At McConnell, a suite of ten frequencies was read between 0.5 and 5 MHz at 0.5-MHz intervals.

Tomographic coverage was 90–170 m in hole 78 930 and 130–310 m in hole 80 578, i.e., in both the hanging wall and footwall of the sulfide deposit (Figure 1b). The transmitter sites were 10 m apart, and the receiver station interval was 2 m.

A center-fed half-wave dipole transmitter with 18-m arms was deployed in hole 78 930 on the first day, but a monopole antenna with a 7-m arm was used in hole 80 578 on the second day. Water infiltration into the transmitter filter pod prompted the change. Signal strength was satisfactory at all frequencies at ranges up to 150 m. The receiver was a monopole, with a 7-m arm, throughout. Analog to digital conversion was affected downhole in the receiver electronics pod, which is 1.2 m long and has an outside diameter of 40 mm.

A limited repeatability test was conducted during ascent of hole 80 578 at the McConnell site, with the transmitter at 30 m depth in hole 78 930 (Figure 1b). The greatest difference in repeat readings was only 0.6 dB at 0.5 MHz. In conjunction with a similar repeatability test performed at other sites, these comparisons engendered confidence in data precision.

The transmitter was operated from each hole in turn to permit a reciprocity test. However, given the change in transmitter and in view of the gradual infiltration of water into the transmitter on the first day, there is no reason to expect reciprocity to apply exactly. The amplitude differences when the positions of the transmitter and receiver were interchanged were indeed substantial, typically between −4 and +4 dB at 5 MHz.

RFEM data reduction and image construction

In RFEM surveys, the amplitude of a single component of either electric or magnetic field is measured at the receiver. To tomographically reconstruct the conductivity structure between boreholes, far-field conditions are assumed. For an electric dipole in a homogeneous and isotropic medium, the received electric field strength in the far-field is given by (Ward and

Hohmann, 1988, p. 173)

$$|E_f(r)| = A_0 e^{\alpha\gamma} \frac{\sin\theta_t \sin\theta_r}{r}, \tag{6}$$

where r is the transmitter-receiver separation, A_0 is the source strength, and θ_t and θ_r are the polar angles of the ray with respect to the transmitter and receiver axes (Figure 2). Treating absorption as an analog for slowness, the apparent attenuation or traveltime, τ_n, for the nth ray is defined by

$$\tau_n = \int_{C_n} \alpha(x, y, z)\, dl, \tag{7}$$

where integration is along the raypath C_n. Taking logarithms of equation (6), it follows from equation (7) that τ can be expressed as

$$\tau = \alpha_a r = -20\log_{10}|E_f| + 20\log_{10} A_0 + 20\log_{10}\left(\frac{\sin\theta_t \sin\theta_r}{r}\right), \tag{8}$$

where α_a is the apparent absorption coefficient in decibels per meter.

The three main sources of error for τ were (1) observational error, (2) uncertainty in A_0, and (3) near-field effects. From our limited repeatability tests, described above, we concluded that observational error is small ($\sim$1 dB). This established data precision but not accuracy.

Generally, A_0 is estimated via analysis of data collected in homogeneous host rocks. After accounting for geometrical effects, A_0 is the intercept on the amplitude versus distance plot. Transmitter sites at depths 130, 140, and 150 m in hole 80 578, far from the massive sulfide contact, were selected for estimation of A_0. After minimum l_1-norm regression (Fullagar et al., 1994), A_0 values of 0.38, 0.38, and 0.40 were obtained for the three transmitter gathers. A starting estimate for the apparent absorption coefficient was computed assuming σ_e was 10^{-4} S/m and ε_r was 6.5 ε_0, in keeping with the best available information for Sudbury resistivities (Mwenifumbo et al., 1993) and permittivities (Fullagar and Livelybrooks, 1994a). The details of the l_1-norm minimization are given by Fullagar et al. (1994). An A_0 value of 0.38 was ultimately adopted.

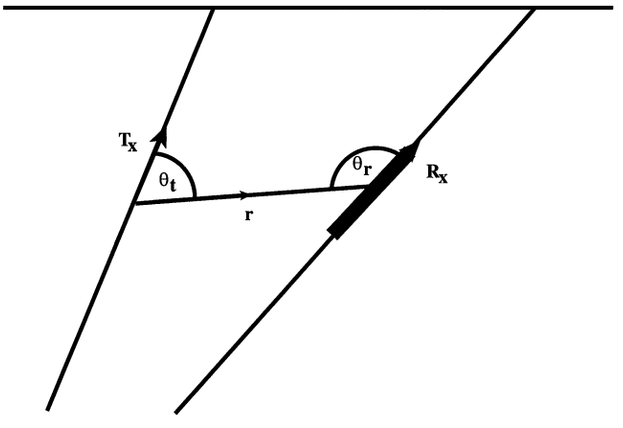

FIG. 2. Crosshole survey schematic, where θ_t and θ_r are the polar ray angles at the transmitter and receiver, respectively.

RFEM transmitter performance is strongly affected in or near sulfide mineralization. Since the transmitter strength is not identical at all locations, its output ideally should be continuously monitored. The JW-4 usually monitors transmitter input current, but this facility was inoperable for the McConnell survey because no suitable three-conductor cables were available on site.

If the source strength is assumed constant, a static shift error is introduced in the tau values at each transmitter site if source strength varies. McGaughey (1990) suggests a simple approach for estimation of such static shifts by enforcing reciprocity. An implementation of this approach is described by Fullagar et al. (1994). It was not applicable at McConnell because reciprocity did not apply. More recently, Cao et al. (1998) proposed frequency differencing as a means to suppress variations in source strength caused by large changes in conductivity near the boreholes. This approach may be suitable for the McConnell data.

Near-field effects can become important as frequency decreases, resistivity increases, path length decreases, or transmitter polar angle decreases (Pears, 1997). To assess the validity of the far-field assumption for the McConnell data, the differences between the full analytic solution and the far-field approximation for an electric dipole in a whole space were compared for transmitters and receivers distributed in space as at McConnell. In a medium with effective of conductivity of 10^{-4} S/m and dielectric constant of 6.5 ε_0, the wavelength at 0.5 MHz is 235 m, larger than the longest raypath at McConnell. Therefore, far-field conditions did not apply at the lower frequencies.

The relative error Δ between far-field and exact amplitudes was computed for an electric dipole in a homogeneous medium, where

$$\Delta = \frac{|E| - |E_f|}{|E|}. \tag{9}$$

For the McConnell survey geometry, the maximum relative error in homogeneous host was estimated to be 5% at 500 kHz. This corresponds to an error of less than 1 dB. The McConnell tomogram presented here corresponds to a frequency of 5 MHz, for which far-field conditions certainly apply.

To invert equation (7), the image plane is discretized and the line integral on the rightside is represented as a summation (e.g., Stewart, 1991). Tomographic reconstruction then reduces to the solution of a system of linear equations for the unknown absorption coefficients within each of the grid cells. Migratom, a SIRT algorithm developed by the U.S. Bureau of Mines (Jackson and Tweeton, 1994), has been used here, assuming straight rays.

To perform a ray-based tomographic reconstruction, it is assumed that the amplitude at the receiver is governed solely by absorption of the signal and that reflection, scattering, and diffraction effects can be ignored. Thus, there is an implicit low-contrast assumption. If a highly conductive body intervenes between the transmitter and receiver, there will be no direct transmission and the inferred absorption coefficient after tomographic reconstruction will not be an accurate indication of the actual absorption coefficient of the conductor.

RFEM interpretation

The absorption tomogram generated from the 5-MHz McConnell data using a modified form of Migratom is presented as Figure 3. The starting model was homogeneous, and clamping weights (Pears and Fullagar, 1998) were applied. Despite the fact that reciprocity is assumed implicitly during tomographic reconstruction, the tomogram based on the full data set was superior (insofar as it provided better definition of the sulfide body) than that obtained when the data acquired with the symmetric transmitter in hole 78 930 were disregarded.

The tomographic reconstruction clearly defines the continuation of the sulfide body over a distance of 110 m between intersections in the two boreholes. However, the inferred absorption is not uniform along the conductor, and irregularities in the contacts appear to be related to the discretization of the image plane.

When the transmitter and receiver are on opposite sides of the sulfide body, the signal amplitude is low but measurable. Propagation of radio signals through a 15-m-thick massive sulfide body is impossible at megahertz frequencies. Nevertheless, the expected radio shadow at McConnell did not eventuate. It was concluded at the time that the signals received on the other side of the conductor either travelled around the edges of the deposit or passed through a gap in the sulfides.

Diffraction around the edges of the sulfide body is a plausible explanation for the relatively high signals since the dimensions of the McConnell deposit (approximately 300×200 m) are comparable to the estimated radio wavelength (230 m) at 500 kHz in the Sudbury Breccia and much larger than the estimated wavelength (22 m) at 5 MHz. To determine whether diffraction alone could explain the observations, 2.5-D finite-difference modeling was performed using the EMSUN program (Smith et al., 1990). The model used to characterize diffraction around the bottom of the slab is depicted in Figure 4. The model conductor is two dimensional (infinite in strike length), but the source is finite (vertical electric dipole). Except for the 2-D limitation, the cross-sectional geometry of the McConnell experiment was replicated as closely as possible for two transmitter positions, T1 and T2, at depths 170 and 190 m in hole 80 578 and two receiver positions, R1 and R2, at depths 108 and 168 m in hole 78 930.

The orebody model was assigned a conductivity of 100 S/m at its core, enclosed within an inner layer of conductivity 1 S/m and an outer layer of conductivity 0.01 S/m. The transitional layers were introduced for numerical stability, since a contrast of 1:100 was regarded as the greatest which could be handled accurately. Geologically, such a transition zone often exists in the form of a disseminated sulfide halo; indeed, at McConnell sulfide is known to occur as blebs in the quartz diorite and as disseminations in the breccia immediately adjacent to the quartz diorite (Grant and Bite, 1984).

The observed and modeled ratios of electric field amplitude at the two receiver sites for the two transmitter positions at 500 kHz are recorded in decibels on Figure 4. For a continuous conductor (no gap), modeling results indicate that after diffraction around the bottom of the slab the signal amplitude is 61 dB lower at R2 on the far side of the conductor than at R1 on the near side for the transmitter at T1 and 54 dB lower

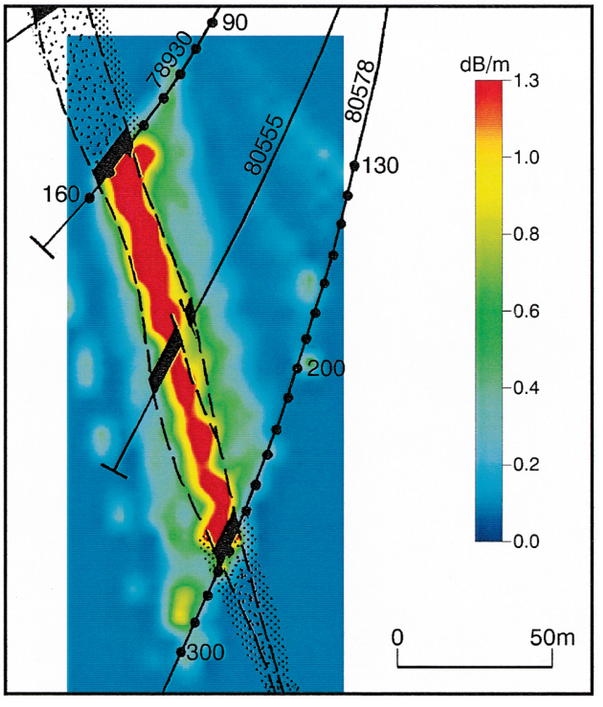

FIG. 3. Radio absorption tomogram at 5 MHz between holes 78 930 and 80 578. Transmitter locations for the RT survey are marked with dots.

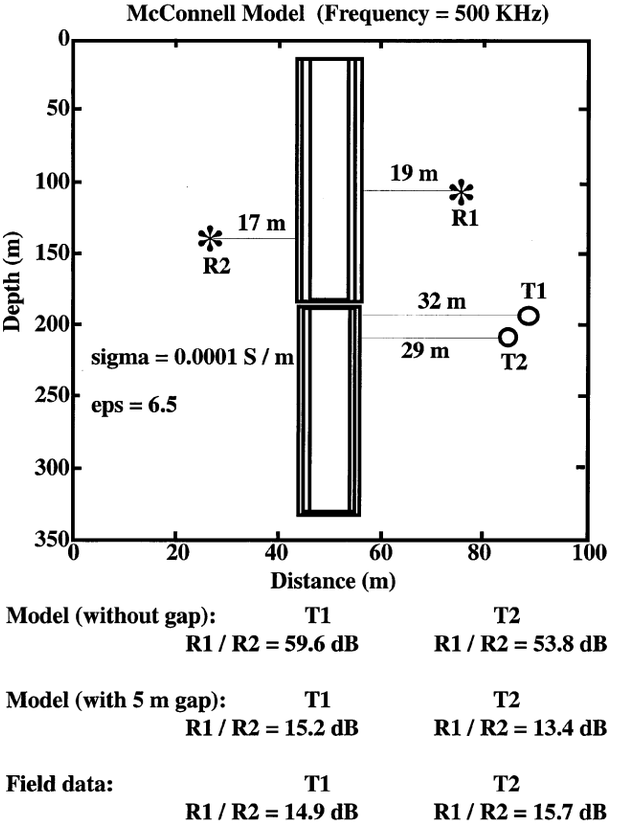

FIG. 4. A 2-D sectional model adopted to investigate diffraction around the bottom of the McConnell deposit.

when the transmitter is at position T2. Even if the signal at R2 is increased by a factor of three to allow for diffraction laterally around the ends of the tabular body, the signal at R2 would still be 51 or 44 dB down relative to that at R1 (note the 15 dB or 16 dB differences observed). Therefore, diffraction around the edges of the deposit cannot fully explain the relatively high field strengths recorded when the transmitter and receiver are on opposite sides of the conductor. Numerical instability precluded 5-MHz modeling; however, at higher frequencies diffraction would be a less effective mechanism.

In light of the modeling, a break (or hole) in the sulfide body was proposed as the explanation for the absence of a shadow (Fullagar et al., 1996). Geologically, there is a hint of a break in continuity of the sulfide in hole 80 555, which passed through a small sulfide interval (188–190 m) and then back into Sudbury Breccia (190–197 m) before passing through the main sulfide interval (Figure 1b). By introducing a 5-m-wide break in the 2-D model in approximately this position, the predicted ratios of near-side to far-side signal amplitudes increase to levels comparable with those observed, even though the gap was a small fraction (~2%) of a wavelength in the breccia at 500 kHz (Figure 4).

More recently, INCO geophysicists have demonstrated that the radio signal strength drops substantially if the metal-cored receiver cable is replaced with reinforced fiber-optic cable (McDowell and Verlaan, 1997). Thus, we now conclude that the JW-4 in-line filters were inadequate to prevent cable pick-up, i.e., that the receiver and transmitter cables were acting as parasitic antennae during the 1994 survey. It is therefore not necessary to invoke a gap or hole in the sulfide body to explain the anomalously high amplitudes in the RT data.

McCONNELL BOREHOLE RADAR

Radar data acquisition and processing

The borehole radar data described here were recorded in 60-mm-diameter boreholes in June 1996 with the Ecole Polytechnique omnidirectional 60-MHz RAMAC LI system. Both single-hole and crosshole configurations were used. The transmitter was positioned automatically using a computer-controlled electric winch.

The RAMAC system is comprised of a control unit connected via optical fibers to a transmitter pulser, amplifier, and antenna and to a receiver antenna, amplifier, trigger, and A/D converter (Olsson et al., 1992). The transmitter antenna emits a short pulse of approximately three half-cycles duration. The received wavetrain for each transmitter–receiver pair is constructed over a window, with only one time sample recorded each time the transmitter fires. For each of 512 time lags, 128 measurements are stacked.

Although the radar data are single fold, the processing has nevertheless been adapted from seismic processing techniques drawn from a number of sources, including Yilmaz (1987), Fisher et al. (1992), Liner and Liner (1995), and Young et al. (1995). Some care must be exercised when borrowing from seismic technology since radar signals exhibit greater attenuation and dispersion than seismic waves.

A dc drift correction, entailing subtraction of the average value for each record prior to the first arrival, was performed on all traces. Subsequent processing steps included spreading and exponential compensatory (SEC) gaining (Annan, 1993), frequency-domain band-pass filtering, and spectral equalization. Processed crosshole reflection radargrams were migrated in an effort to delineate radar reflectors.

Radar tomography

Crosshole 60-MHz radar data were acquired between boreholes 78 930 and 78 929 in 1996. For each of 18 transmitter positions in hole 78 929, data were recorded at 25 receiver depths in hole 78 930. Transmitter and receiver spacings were both 2.5 m, comparable to the expected radar wavelength. The crosshole survey was originally designed to image the radar velocity and attenuation above the ore deposit, primarily to gauge the absorption and velocity heterogeneity of the Sudbury Breccia. The scanning pattern is not suitable for imaging the ore boundaries.

Straight-ray tomographic inversion of first-arrival times was performed using Migratom. The velocity tomogram (Figure 5a) reveals a fairly high degree of heterogeneity within the breccia. A lobe of low velocity extending down from hole 78 929 toward hole 78 930 may correspond to the low-resistivity zones defined in the borehole logs: 88–95 m in 78 929 and 114–118 m in 78 930 (Figure 6). The low velocity and low resistivity might indicate water-filled fractures.

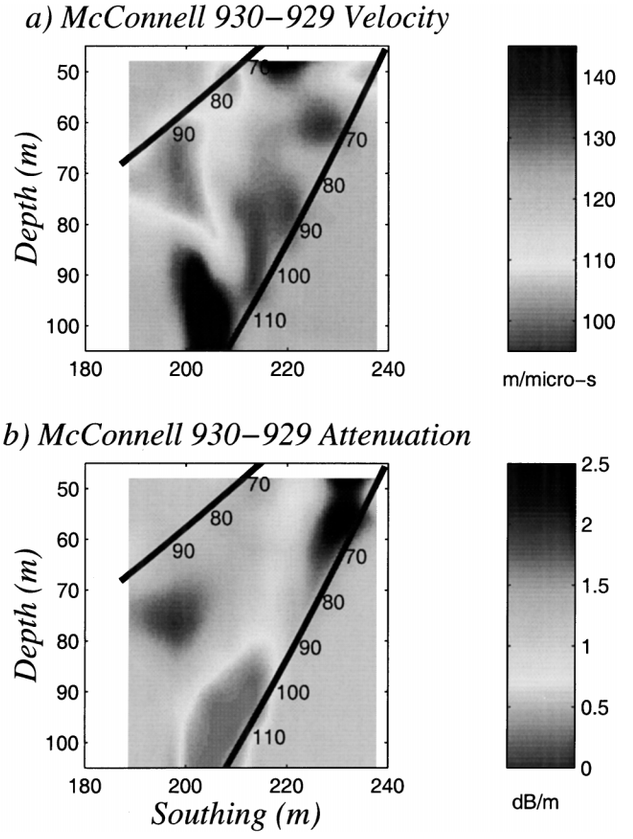

FIG. 5. (upper) Hanging-wall radar velocity tomogram between boreholes 78 929 and 78 930. Text gives details regarding the tomographic inversion process. Radar velocities are in meters per microsecond. (lower) Radar absorption tomogram for the same region. Absorption coefficient in decibles per meter.

First-arrival amplitudes were corrected for spherical spreading and for a dipolar radiation pattern, as per equation (8), prior to SIRT reconstruction. The resulting absorption tomogram is shown in Figure 5b. The radar absorption coefficient in the breccia is typically 1 dB/m at 60 MHz. In general, velocity (ω/β) and absorption are anticorrelated, as expected from equations (1) and (2), when attenuation is appreciable.

Single-hole reflection GPR imaging

The 1996 single-hole reflection surveys were undertaken in holes 78 929 and 78 930. The transmitter and receiver were separated by 4.7 m. Coverage was from 75 to 130 m in hole 78 929 and from 75 to 170 m in hole 78 930 at a station spacing of 0.25 m. The center frequency of the received radar signals was approximately 48 MHz.

An SEC gain was applied to the radargrams. A velocity of 125 m/μs (the average from the velocity tomogram) and an absorption coefficient of 0.75 dB/m (based on the attenuation rate of trace envelopes) were adopted to specify the gain function. A band-pass filter with corner frequencies of 30 and 75 MHz was applied to all traces to suppress long-period fluctuations and late-time drift. Spectral equalization (Young et al., 1995), which flattens the spectrum in a manner akin to deconvolution, was also applied.

Reflection data were recorded above, within, and below the massive sulfide mineralization, and data amplitudes vary markedly. The resulting radargrams for boreholes 78 929 and 78 930 are presented in raw and processed form in Figure 6, with geology and resistivity logs (Mwenifumbo et al., 1993). The resistivity logs are clipped at around 30 000 ohm-m because of loss of sensitivity (negligible current).

A clear radar reflection from the massive sulfide hanging-wall contact was observed in hole 78 929 (Figure 6a). However, there is no obvious reflection from the footwall contact in 78 929 nor from either contact in hole 78 930 (Figure 6b). This was a surprising and, from a practical viewpoint, disappointing observation. The main factors responsible for the absence of reliable reflections are probably (1) unfavorable endfire orientation of the antennae with respect to the contact, (2) heterogeneity of the breccia, (3) local irregularity of the sulfide contact, and (4) minor concentrations of disseminated sulfide in and immediately adjacent to the quartz diorite.

There is total extinction of signal when either antenna is within the sulfide body. In addition, there are highly absorptive intervals and zones of low resistivity in the hanging wall in both holes. The correlation between low resistivity and low radar amplitude is by no means perfect as plotted in Figure 6, but a depth shift of approximately 5 m would achieve a close correspondence. A systematic depth error in one or the other data set is suspected.

The combination of SEC gain and spectral equalization recovered interpretable signal in the low-amplitude intervals. The intervals of high absorption within the breccia are not correlated with lithology and may signify fluid-filled fracture zones. Weak reflections, coherent for tens of meters, can be discerned elsewhere in the breccia. These are presumably from fractures or lithological boundaries.

Crosshole radar reflection

The crosshole first arrivals carry little or no information on the deposit geometry. However, an attempt has been made to focus crosshole reflections from the sulfide contact into an image via migration (Calvert and Livelybrooks, 1997).

The survey geometry is unfavorable for reception of reflections from the sulfide, given that the dipole antennae are in almost endfire orientation with respect to the hanging-wall contact (Figure 1b). Reflection amplitudes would be further reduced by attenuation when one or both of the antennae are far from the sulfide contact. When both transmitter and receiver antennae are close to the sulfides, the reflection from the contact would be difficult to distinguish from the direct arrival. Survey geometry also dictates that any crosshole reflections from the contact will originate from a relatively small area straddling the point where hole 78 929 pierces the sulfide body (Bellefleur and Chouteau, 1998). From a practical viewpoint, therefore, the analysis of crosshole reflections is destined to provide limited new information about the shape of the contact.

After suppression of the direct arrivals and application of geometric spreading correction, the data were migrated using a 2-D Kirchhoff-style algorithm. A constant velocity of 105 m/μs was assumed. The migrated data are depicted in Figure 7.

Reflective zones between the boreholes have been identified. Those in midpanel, near true depth 60 m, could be from lithological contrasts within the breccia. Of greater interest is the inferred reflectivity trend paralleling the sulfide contact. Given the assumptions underlying the migration (2-D geometry, constant velocity, spherical radiation pattern), this result is reasonably encouraging. The recording window was only 623 ns; some improvement could be expected if data were recorded over a longer interval.

Bellefleur and Chouteau (1998) have achieved an improved result migrating these same data by (1) restricting reflector dip to a particular range, (2) suppressing down-going waves, and (3) adopting the velocity tomogram as the migration velocity model. In their migrated image, the strongest reflection is coincident with the sulfide contact.

DISCUSSION

Investigation of the efficacy of radio tomography and borehole radar for delineation of massive sulfide bodies commenced at McConnell in 1993. The impetus for the research was the need for accurate geophysical definition of ore contacts, both during near- and in-mine exploration and for orebody delineation.

Radio frequency tomography with a JW-4 electric dipole system successfully imaged the McConnell sulfide deposit over a down-dip distance of 110 m. Data were recorded at ten frequencies between 0.5 and 5.0 MHz. Signals propagated over 150 m through Sudbury Breccia host rock, even at 5 MHz. The sulfide deposit shape was well defined on the resulting tomogram as a zone of high absorption. Thus, the first RT survey at McConnell demonstrated the potential of radio imaging to map sulfide bodies in highly resistive host rocks. The results were sufficiently encouraging to prompt further RT investigations in the Sudbury area by INCO (McDowell and Verlaan, 1997) and, more recently, by Falconbridge (Stevens and Redko, 2000).

There was complete extinction of radio signal when either antenna was located within the massive sulfides. However, signal amplitudes were considerably stronger than expected when the transmitter and receiver were on opposite sides of the sulfide body. The 2.5-D modeling indicated that diffraction around the edges of the conductor was inadequate to explain the observed signal levels, and the conclusion at the time pointed to a break in continuity of the sulfides. According to the modeling, a 5-m-wide gap is compatible with the observed data. A break or hole in the mineralization had not been previously interpreted geologically, though two mineralized intervals had been intersected in hole 80 555 and interpreted as a reentrant (Figure 1b).

The transmitter and receiver cables were copper cored (two-conductor) and could therefore have served as parasitic antennae. Although the JW-4 system included a filter to isolate the receiver, investigations by INCO since the original experiment have confirmed that the 1994 data were affected by cross-cable pick-up. The potential of radio imaging to detect narrow gaps in conductors remains an interesting possibility, but there is no

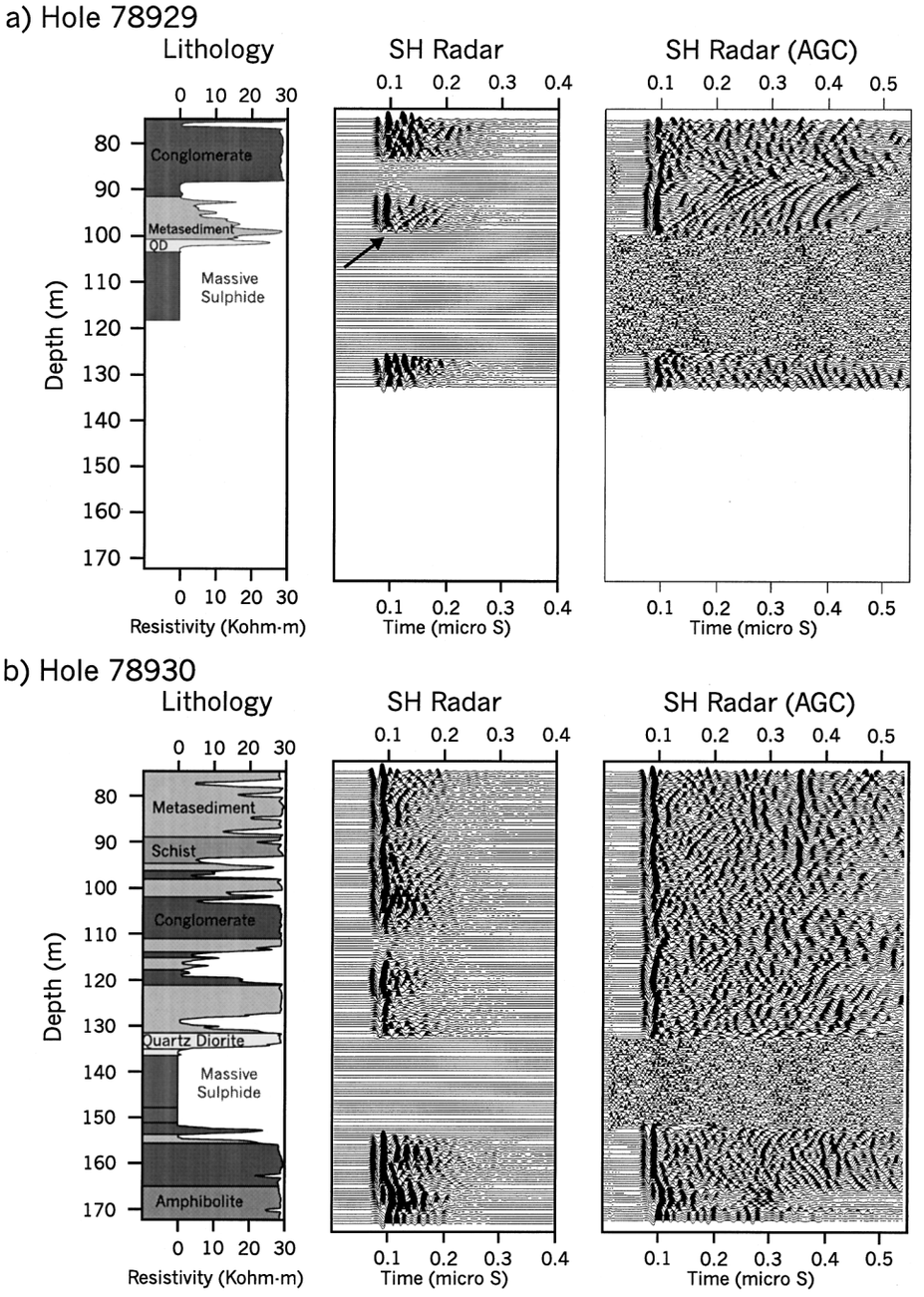

FIG. 6. Two 60-MHz single-hole reflection radargrams, without and with AGC, for boreholes (a) 78 929 and (b) 78 930 (after Calvert and Livelybrooks, 1997). Resistivity logs (Mwenifumbo et al., 1993) shaded according to lithology, shown at left.

longer any reason to invoke the existence of a gap to explain the 1994 McConnell RT data.

GPR, especially in reflection mode, offers the potential for high-resolution mapping of geological contacts and structures. The single-hole borehole radar reflection surveys at McConnell in 1993 and 1996 demonstrated that the sulfide contacts only sometimes produce strong coherent reflections. The main factors responsible for the erratic occurrence of clear reflections are probably (1) unfavorable endfire geometry, which reduces the S/N ratio, (2) heterogeneity of the host breccia, (3) minor concentrations of disseminated sulfide in or immediately adjacent to the quartz diorite, and (4) local irregularity of the sulfide contact. Of these, only the first can be altered. Borehole radar would be far more likely to succeed in holes drilled parallel to the sulfide contact, permitting broadside illumination of the target. This exposes the contradistinction between the geophysical view of drillholes as accessways for instruments and the geological view of drillholes, as voids created during sampling. Purpose-drilled holes for borehole radar represent an additional survey cost; on the basis of the results obtained to date, it is unclear whether the additional expense would be justified at McConnell.

The crosshole GPR survey between boreholes 78 929 and 78 930 was suitable for tomographically imaging velocity and absorption coefficient in the breccia above the orebody. The velocity within the breccia exhibited significant variation, ranging between 95 and 145 m/μs and averaging about 125 m/μs. The absorption coefficient ranged up to 2.5 dB/m, averaging 1.2 dB/m. The crosshole tomography thus confirmed that the breccia is appreciably heterogeneous and hence less favorable for radar propagation than its high resistivity might suggest. For $\alpha = 1.2$ dB/m $= 0.14$ neper/m and $v = 125$ m/μs, it follows that $Q \approx 11$ in the Sudbury Breccia. Although derived from 60-MHz data, this Q value could be reasonably characteristic of the breccia at all radar frequencies since conductivity is approximately proportional to frequency for many materials (Johnscher, 1977), while the real part of permittivity is often only weakly dependent on frequency (Collett and Katsube, 1973).

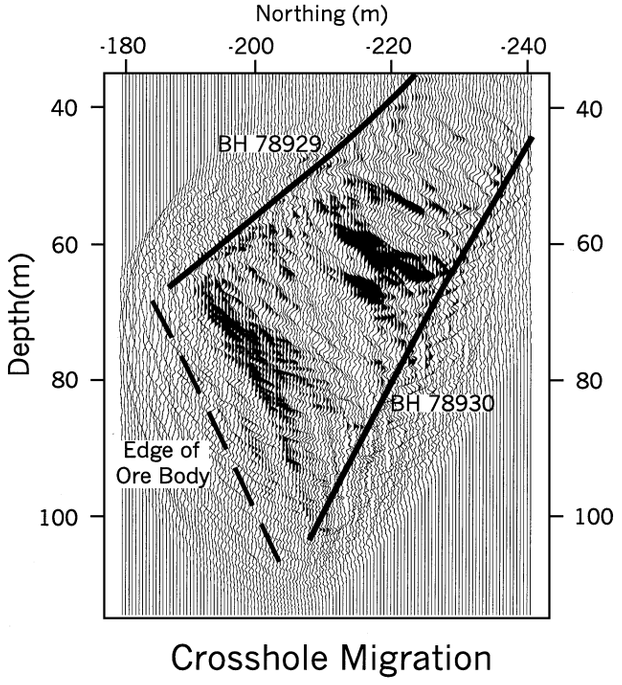

FIG. 7. Kirchhoff-style migration of crosshole radar data for the region between boreholes 78 929 and 78 930. Text gives details regarding data processing and migration. The geologically inferred location of the McConnell orebody is also outlined for reference (after Calvert and Livelybrooks, 1997).

Migration of crosshole reflection data has defined a reflectivity feature which lies above and parallel to the contact. While a worthwhile technical achievement, the migration of McConnell data was destined never to greatly advance the knowledge of the contact geometry, given that reflections originate near where hole 78 929 pierces the contact. However, in another situation, between parallel boreholes drilled orthogonal to a contact, migration of crosshole reflection could yield valuable information.

CONCLUSIONS

Radio imaging is a potentially effective means for imaging massive sulfide orebodies in resistive environments. Specifically,

1) RT surveys depict orebodies as zones of enhanced attenuation;
2) radio imaging uses lower frequencies than GPR, thereby achieving greater range but lower resolution;
3) RFEM is less sensitive to the presence of disseminated sulfide;
4) the absence of a physical link between transmitter and receiver is a significant logistical advantage in mining environments; and
5) typically, RFEM data can be collected more rapidly than GPR, since finer spatial sampling is required for GPR. Recording times for both RFEM and GPR could be slashed using multichannel acquisition systems.

The advantages and disadvantages of single-hole reflection radar can be summarized as follows:

1) radar reflection surveys offer greater resolution but smaller range than either radio imaging or crosshole radar;
2) both transmitter and receiver are in the same borehole, so data acquisition is uncomplicated and efficient;
3) radar reflection data are amenable to seismic processing, a highly developed technology;
4) reflection radar is sensitive to heterogeneity in the host rock and to the presence of even minor concentrations of disseminated sulfide; and
5) unless dip and strike are known a priori, or unless directional antennae are deployed, surveys in more than one hole are required to overcome rotational ambiguity.

Crosshole GPR surveying shows some promise for imaging ore boundaries. Its strengths and weaknesses are

1) times and amplitudes of first arrivals can be used to image interhole velocity and absorption;
2) direct arrivals can be distinguished from reflections and diffractions;

3) later reflections can potentially be migrated to define strong reflectors;
4) larger data volumes and more elaborate processing add to the cost of crosshole GPR; and
5) the need for a physical connection between the transmitter and receiver limits applicability, especially underground.

ACKNOWLEDGMENTS

This work was completed under the auspices of the NSERC/TVX Gold/Golden Knight Chair in Borehole Geophysics for Mineral Exploration, Department of Mineral Engineering, Ecole Polytechnique, Montreal, Canada.

The McConnell surveys were jointly funded by INCO Ltd. and Noranda; their support is gratefully acknowledged. Data acquisition was expedited by the efforts of many INCO personnel, while Alan King and Gord Morrison assisted with planning and interpretation. The data have been released for publication by the kind permission of Larry Cochrane of INCO Ltd., Ontario.

The Migratom tomographic software was provided by Daryl Tweeton and Michael Jackson (U.S. Bureau of Mines, Minneapolis). The EMSUN modeling program was made freely available by Keeva Vozoff (Harbourdom, Sydney, Australia). Geoff Smith (Univ. of Technology, Sydney, Australia) assisted with the EMSUN modeling.

The 1993 borehole radar data were recorded by an AECL crew, led by Kevin Stevens. The 1994 radio imaging data were recorded by Wu Yiren, Qu Xingchang, and Zhang Ziling from the Chinese Ministry of Geology and Mineral Resources (MGMR), Beijing. Maree-Josee Bertrand, Noranda, assisted with interpretation of the radio imaging data.

The paper benefitted from comments by Greg Turner and an anonymous reviewer. Mike Asten is to be commended for his editorial persistence and patience.

REFERENCES

Anderson, C. G., and Logan, K. J., 1992, The history and current status of geophysical exploration at the Osborne Cu and Au deposit, Mt. Isa: Expl. Geophys., **23**, 1–8.

Annan, A. P., 1993, Practical processing of GPR data: 2nd Govt. Workshop on GPR, Proceedings, 1–22.

Bellefleur, G., and Chouteau, M., 1998, Borehole radar and delineation of the McConnell massive sulfide deposit, Sudbury, Ontario: 7th Internat. Conf. on Ground Penetrating Radar Proceedings, 353–358.

Calvert, A. J., and Livelybrooks, D., 1997, Borehole radar reflection imaging at the McConnell nickel deposit, Sudbury: Exploration '97, 4th Decennial Internat. Conf. on Min. Expl., Proceedings, 701–704.

Campbell, G., 1994, Geophysical contributions to mine development planning—A risk reduction approach: 15th CMMI Congress, S. African Inst. Min. Metall., **3**, 283–325.

Cao, J., Nie, Z., and Zhu, J., 1998, Dual frequency conductivity tomography: 4th Soc. Expl. Geophys. Japan Internat. Symp., Proceedings, 227–230.

Collett, L. S., and Katsube, T. J., 1973, Electrical parameters of rocks in developing geophysical techniques: Geophysics, **38**, 76–91.

Cook, J. C., 1975, Radar transparencies of mine and tunnel rocks: Geophysics, **40**, 865–875.

Coon, J. B., Fowler, J. C., and Schafers, C. J., 1981, Experimental uses of short pulse radar in coal seams: Geophysics, **46**, 1163–1168.

Davis, J. L., Annan, A. P., and Vaughan, C. J., 1985, Placer exploration using radar and seismic methods: Can. Inst. Min. Bull., **80**, 60–72.

Eisenburger, D., Sender, F., and Thierbach, R., 1993, Borehole radar—An efficient geophysical tool to aid in the planning of salt caverns and mines: 7th Internat. Symp. on Salt, **1**, 279–284.

Fisher, E., McMechan, G. A., Annan, A. P., and Cosway, S. W., 1992, Examples of reverse-time migration of single-channel ground-penetrating radar profiles: Geophysics, **57**, 577–586.

Fullagar, P. K., and Livelybrooks, D., 1994a, Trial of tunnel radar for cavity and ore detection in the Sudbury mining camp, Ontario: 5th Internat. Conf. on Ground Penetrating Radar, Proceedings, **3**, 883–894.

——— 1994b, NSERC/TVX Gold/Golden Knight Chair in Borehole Geophysics for Mineral Exploration annual report: Ecole Polytechnique de Montreal, Department of Mineral Engineering.

Fullagar, P. K., Zhang, P., and Wu, Y., 1994, Trial of radio tomography for exploration and delineation of massive sulfide deposits in the Sudbury Basin: Ecole Polytechnique de Montreal, Department of Mineral Engineering.

Fullagar, P. K., Zhang, P., Wu, Y., and Bertrand, M.-J., 1996, Application of radio frequency tomography to delineation of nickel sulfides in the Sudbury basin: 66th Ann. Internat. Mtg., Soc. Expl. Geophys., Extended Abstracts, 2065–2068.

Grant, R. W., and Bite, A., 1984, Sudbury quartz diorite offset dikes, *in* Pye, E. G., Naldrett, A. J., and Giblin, P. E., Eds., The geology and ore deposits of the Sudbury structure: Ontario Ministry of Natural Resources, 275–300.

Jackson, M., and Tweeton, D., 1994, MIGRATOM—Geophysical tomography using wavefront migration and fuzzy constraints: U.S. Bureau of Mines Report of Investigations RI 9497.

Johnscher, A. K., 1977, The 'universal' dielectric response: Nature, **267**, 673–679.

Killeen, P., Mwenifumbo, C., and Elliott, B., 1996, Mineral deposit signatures by borehole geophysics—Data from the borehole geophysical test at the McConnell nickel deposit (Garson offset), Ontario: Natural Resources Canada, Geological Survey of Canada, Open file report 2811.

King, A., 1996, Deep drillhole electromagnetic surveys for nickel/ copper sulfides at Sudbury, Canada: Expl. Geophys., **27**, 105–118.

Lager, D. L., and Lytle, R. J., 1977, Determining a subsurface electromagnetic profile from high frequency measurements by applying reconstruction technique algorithms: Radio Sci., **12**, 249–260.

Liner, C. L., and Liner, J. L., 1995, Ground-penetrating radar: A near-face experience from Washington County, Arkansas: The Leading Edge, **14**, 17–21.

Liu, Q., Osman, N., Manning, P., Hargreaves, J., Mason, I., and Turner, G., 1998, Borehole radar reflection characteristics of nickel sulfide shoots: Australian Mining Tech. Conf., Proceedings, 333–346.

McDowell, G., and Verlaan, L., 1997, Radio imaging for sulfide orebody delineation: High-Res. Geophys. Workshop, Dept. of Mining and Geol. Eng., The University of Arizona, Proceedings.

McGaughey, W. J., 1990, Mining applications of crosshole seismic tomography: Ph.D. thesis, Queen's Univ.

McGaughey, W. J., and Stolarczyck, L. G., 1991, Tomographic inversion of EM seam-wave absorption in the Prairie Evaporite Formation, Saskatchewan: 61st Ann. Internat. Mtg., Soc. Expl. Geophys., Expanded Abstracts, 403–406.

Mundry, E., Thierbach, R., Sender, F., and Weichart, H., 1983, Borehole radar probing in salt deposits: 6th Internat. Symp. on Salt, **1**, 585–599.

Murray, W., Williams, C., Lewis, C., and Hatherly, P., 1998, Development of geophysical logging and imaging tools for use in in-seam drilling: Australian Mining Tech. Conf., Proceedings, 327–332.

Mwenifumbo, C. J., Killeen, P. G., Elliott, B. E., and Pflug, K. A., 1993, The borehole geophysical signature of the McConnell nickel deposit, Sudbury area: 5th Internat. Symp., Min. and Geotech. Logging Soc., Proceedings.

Nickel, H., and Cerny, I., 1989, More effective underground exploration for ores using radio waves: Expl. Geophys., **20**, 371–377.

Olsson, O., Falk, L., Forslund, O., Lundmark, L., and Sandberg, E., 1990, Crosshole investigations—Results from borehole radar investigations (revised 1990, original report 1987): Stripa Project technical report **87-11**.

Pears, G. A., 1997, Tomography-based AIM inversion of radio frequency electromagnetic data: M.S. thesis, Univ. of Queensland.

Pears, G. A., and Fullagar, P. K., 1998, Weighted tomographic imaging of radio frequency data: Expl. Geophys., **29**, 554–559.

Qu, X., Gao, W., and Zhou, H., 1991, JW-4 subsurface electromagnetic meter: Presented at Conf. on Appl. of Computing Tech. in Geosci.

Raadsma, J. M., 1994, Ground penetrating radar applications on high grade gold deposits at the Sixteen to One Mine, California: 5th Internat. Conf. on Ground Penetrating Radar, Proceedings, **3**, 925–940.

Smith, G. H., Williamson, P. R., and Vozoff, K., 1990, The application of nested dissection to the solution of a 2.5D electromagnetic problem: Appl. Computat. Electromag., **5**, 87–106.

Stevens, K. M., and Lodha, G. S., 1994, Borehole radar surveys at the McConnell deposit—Garson offset, Sudbury, Ontario: Appl. Geophys. Branch, Atomic Energy of Canada, Ltd., Pinawa, Manitoba, AECL Reference #008263-002.

Stevens, K., and Redko, G., 2000, In-mine applications of the radio wave method in the Sudbury igneous complex: 70th Ann. Internat. Mtg., Soc. Expl. Geophys., Expanded Abstracts, (in press).

Stewart, R. D., and Unterberger, R. R., 1976, Seeing through rock salt with radar : Geophysics, **41**, 123–132.
Stewart, R. R., 1991, Exploration seismic tomography—fundamentals, *in* Domingo, S. N., Ed., Course notes series, **3**, Soc. Expl. Geophys.
Thierbach, R., 1994, Twenty years of ground-probing radar in salt and potash mines: 5th Internat. Conf. on Ground Penetrating Radar, Proceedings, **3**, 957–980.
Thomson, S., and Hinde, S., 1993, Bringing geophysics into the mine: Radio attenuation imaging and mine geology: Expl. Geophys., **24**, 805–810.
Thomson, S., Young, J., and Sheard, N., 1992, Base metal applications of the radio imaging method—current status and case studies: Expl. Geophys., **23**, 367–372.
Turner, G., and Siggins, A. F., 1994, Constant Q attenuation of subsurface radar pulses: Geophysics, **59**, 1192–1200.
Vozoff, K., Smith, G. H., Hatherly, P. J., and Thomson, S., 1993, An overview of the radio imaging method in Australian coal mining: First Break, **11**, 13–21.
Ward, S. H., and Hohmann, G. W., 1988, Electromagnetic theory for geophysical applications, *in* Nabighian, M. N., Ed., Electromagnetic methods in applied geophysics **1**, Theory: Soc. Expl. Geophys., Investigations in Geophysics **3**, 131–311.
Wedepohl, E., 1993, Radio wave tomography-imaging ore bodies using radio waves: 3rd Tech. Mtg., South African Geophys. Assn., Expanded Abstracts, 85–88.
Wedepohl, E., Trickett, J., van Schoor, M., Grodner, M., and Schweitzer, J., 1998, A geophysical toolbox for deep level gold mining, South Africa: Australian Mining Tech. Conf., Proceedings, 269–291.
Yelf, R., Turner, G., Hatherly, P., and Hagen, D., 1990, Appraisal of ground penetrating radar in underground coal mines: Final Report for NERDDC Project 1210, Australian Coal Industry Research Laboratories.
Yilmaz, O., 1987, Seismic data processing: Soc. Expl. Geophys.
Young, R., Deng, Z., and Sun, J., 1995, Interactive processing of GPR data: The Leading Edge, **14**, 275–280.
Zhou, B., and Fullagar, P. K., 2000, Borehole radar conductivity and permittivity tomography: 8th Internat. Conf. on Ground Penetrating Radar, Proceedings (in press).
Zhou, B., Fullagar, P. K., and Fallon, G. N., 1998, Radio frequency tomography trial at Mt. Isa mine: Expl. Geophys., **29**, 675–679.